CrossMark

# Study of a novel rapid vacuum pressure swing adsorption process with intermediate gas pressurization for producing oxygen

Xianqiang Zhu[1,3] · Yingshu Liu[1,2] · Xiong Yang[1] · Wenhai Liu[1]

**Abstract** A novel rapid vacuum pressure swing adsorption process with intermediate gas pressurization for producing oxygen is proposed to improve the performance of miniature oxygen concentrator based rapid pressure swing adsorption technology. The effects of intermediate gas pressurization and desorption pressure on the performance of the process are evaluated by experiments and simulations. Results showed that pressurization with intermediate gas from product end can effectively improve the oxygen purity of the product. The pressure and oxygen purity of intermediate gas before pressurization were key parameters that affected the oxygen purity of the product. When the adsorption pressure was 240 kPa and the desorption pressure was 60 kPa, the test unit for the process produced 0.75 L min$^{-1}$ of $\sim$90% O$_2$ with 29.45% of oxygen recovery from compressed air. The minimum bed size factor (BSF) for $\sim$90% O$_2$ product was 82.84 kg TPD$^{-1}$. The BSF could be effectively reduced by lowering the desorption pressure. Moreover, oxygen recovery could be improved by lowering the desorption pressure.

✉ Yingshu Liu
  ysliu@ustb.edu.cn

1   School of Energy and Environmental Engineering, University of Science and Technology Beijing, Beijing 100083, China

2   Beijing Key Laboratory of Energy Saving and Emission Reduction for Metallurgical Industry, University of Science and Technology Beijing, Beijing 100083, China

3   Jiangsu Oxtek Air Equipment & Technology Co., Ltd., Danyang 212300, China

## List of symbols

**Latin letters**

| | |
|---|---|
| $b_i$ | Langmuir parameter (kPa$^{-1}$) |
| $b_i^0$ | Langmuir parameter (kPa$^{-1}$) |
| $c$ | Molar concentration (mol m$^{-3}$) |
| $c_i$ | Component $i$ molar concentration (mol m$^{-3}$) |
| $C_f$ | Gas heat capacity (J kg$^{-1}$ K$^{-1}$) |
| $C_s$ | Solid heat capacity (J kg$^{-1}$ K$^{-1}$) |
| $d_p$ | Particle diameter (m) |
| $d_{in}$ | Column diameter (m) |
| $D_{ax}$ | Axial dispersion coefficient (m$^2$ s$^{-1}$) |
| $D_e$ | Effective lumped diffusivity (m$^2$ s$^{-1}$) |
| $D_m$ | Molecular diffusion coefficient (m$^2$ s$^{-1}$) |
| $D_K$ | Knudsen diffusivity (m$^2$ s$^{-1}$) |
| $l$ | Nitrogen adsorbents loading height (m) |
| $L$ | Column height (m) |
| $Nu$ | Nusselt number |
| $h_f$ | Gas–solid heat transfer coefficient (W m$^{-2}$ K$^{-1}$) |
| $h_w$ | Internal gas-wall convective heat transfer coefficient (W m$^{-2}$ K$^{-1}$) |
| $k_i$ | LDF mass transfer coefficient for adsorbate $i$ (s$^{-1}$) |
| $K_f$ | Gas thermal dispersion coefficient (W m$^{-1}$ K$^{-1}$) |
| $K_s$ | Solid phase thermal conductivity (W m$^{-1}$ K$^{-1}$) |
| $P$ | Pressure (kPa) |
| $P_i$ | Gas partial pressure (kPa) |

| $P_H$ | Adsorption pressure (kPa) |
|---|---|
| $P_L$ | Desorption pressure (kPa) |
| $P_{RE}$ | Pressure at end of RE step (kPa) |
| $P_{IPP}$ | Pressure at end of IPP step (kPa) |
| $Pe_\infty$ | Limiting Peclet number |
| $Pr(=\mu C_f / K_f)$ | Prandtl number |
| $q_0/c_0$ | Dimensionless Henry's law constant |
| $q_i$ | Adsorbed concentration of the component $i$ (mol kg$^{-1}$) |
| $q_i^*$ | Equilibrium adsorption concentration of the component $i$ (mol kg$^{-1}$) |
| $q_s$ | Saturation adsorbed concentration (mol kg$^{-1}$) |
| $R$ | Gas constant (J mol$^{-1}$ K$^{-1}$) |
| $Re(=d_p \rho_f u / \mu)$ | Reynolds number |
| $S_{12}$ | Adsorbent selectivity |
| $t$ | Time (s) |
| $t_C$ | Cycle time (s) |
| $T$ | Temperature (K) |
| $T_f$ | Gas temperature (K) |
| $T_F$ | Feed temperature (K) |
| $T_{RE}$ | Intermediate gas temperature (K) |
| $T_s$ | Solid temperature (K) |
| $T_w$ | Wall temperature (K) |
| $u$ | Interstitial gas velocity (m s$^{-1}$) |
| $u_{in}$ | Feed velocity (m s$^{-1}$) |
| $y$ | Oxygen purity of gas |
| $y_F$ | Oxygen purity of feed gas |
| $y_{RE}$ | Oxygen purity of intermediate gas |
| $z$ | Axial position (m) |

**Greek letters**

| $\mu$ | Dynamic viscosity (Pa s) |
|---|---|
| $\rho_f$ | Gas density (kg m$^{-3}$) |
| $\rho_p$ | Apparent density (kg m$^{-3}$) |
| $\rho_b$ | Bulk density (kg m$^{-3}$) |
| $\varepsilon_b$ | Inter-particle porosity |
| $\varepsilon_p$ | Particle porosity |
| $\varepsilon_t$ | Total bed porosity |
| $\gamma_1$ | Axial tortuosity factor |
| $\tau_p$ | Pore tortuosity |
| $\Delta H_i$ | Heat of adsorption (J mol$^{-1}$) |

# 1 Introduction

Rapid pressure swing adsorption (RPSA) is characterized by short cycle time and high productivity, and this process is particularly suitable for miniature medical oxygen concentrators (Rama Rao et al. 2010; Chai et al. 2011; Rama Rao and Farooq 2014). The traditional RPSA process typically consists of two steps: adsorption and desorption. However, the simplicity of the process leads to a low oxygen purity (average oxygen molar fraction of the product) and poor oxygen recovery (moles of $O_2$ in product/moles of $O_2$ in feed air/cycle) of traditional RPSA process product (Sircar and Hanley 1995). To further improve RPSA performance, the effects of particle size (Alpay et al. 1994; Rama Rao et al. 2014a), rapid pressurization and column length to diameter ratio (Rama Rao et al. 2014a), rapid desorption (Chai et al. 2012, 2013; Rama Rao et al. 2014a, b), pressure drop (Rama Rao et al. 2014a), radial flow (Huang and Chou 2003), and other parameters (Rama Rao et al. 2015a) on the RPSA process were numerically evaluated. The results showed that pressure drop, mass transfer resistance and non-isothermal characteristics significantly influence RPSA performance. Then, an experimental mini-RPSA setup (Chai et al. 2011) was established to investigate the reduced degree of the bed size factor (Leavitt 1991) [BSF, kg of adsorbent in the pressure swing adsorption (PSA) unit per ton of contained $O_2$ per day production rate (TPD)] by lowering the cycle time. Results showed that a BSF of 10–25 kg TPD$^{-1}$ to produce $\sim$90% $O_2$ can be achieved, and the adsorber size can potentially be reduced by a factor of 3–4. Consequently, Rama Rao et al. (2014c) constructed a larger RPSA cyclic test unit consisting of a single adsorber enclosed inside a product storage tank. In addition, the effects of different adsorbents (Rama Rao et al. 2015b) and feed pressure (Rama Rao et al. 2015c) on the performance of a medical oxygen concentrator using RPSA technology were experimentally studied. When the adsorption pressure was 400 kPa and the desorption pressure was 100 kPa, the minimum BSF with an oxygen recovery of $\sim$25% was 43.86 kg TPD$^{-1}$ (Rama Rao et al. 2015c). This performance indicated that a truly compact and portable medical oxygen concentrator can be manufactured by applying RPSA. However, rapid cycling with high adsorption pressure may induce higher gas velocity, thereby possibly intensifying agglomeration and fluidization of adsorbent (Lopes et al. 2012), particularly for adsorbents with small particles, and ultimately affecting the stability of the oxygen concentrator (Liu et al. 2014). A rapid vacuum pressure swing adsorption (RVPSA) design may weaken the adverse effects and exhibit better performance.

The development of miniature air vacuum compression technology (Drevitson et al. 2007; Hu et al. 2009) offered several possibilities for the RVPSA process. The application of air integrated vacuum and compressor in RVPSA system is beneficial to improve the portability of the oxygen concentrator. More importantly, the portable medial oxygen concentrator based PSA technology has been widely used at high altitudes to relieve hypoxia in recent years (Windsor and Rodway 2006; Shen et al. 2012, 2013). The RVPSA

process would exhibit advantages at high altitudes because of the low barometric pressure. However, publications that reported experimental performance of RVPSA oxygen generating systems were scarce.

A novel RVPSA process with intermediate gas pressurization was proposed in this work for application as a miniature oxygen concentrator. The effects of intermediate gas pressurization step and desorption pressure on the performance of the process were investigated by experiments and simulations.

## 2 Experimental section

### 2.1 Materials

LiLSX adsorbents were provided by Luoyang Jianlong Micro-nano Novel Materials Co., LTD (in China). Some physical properties of LiLSX pellets are shown in Table 1. The adsorption isotherms of LiLSX pellets were measured in our laboratory apparatus using a high pressure volumetric apparatus up to 350 kPa, where the adsorption isotherms of pure $O_2$ and $N_2$ on LiLSX pellets were measured at two different temperatures (291.15 and 303.15 K). Adsorbents were regenerated overnight at 573.15 K before being used in measurements.

### 2.2 Process description

The countercurrent back purge step was generally designed to improve oxygen purity of the product in traditional PSA process (Ruthven 1984; Rege and Yang 1997). However, the countercurrent back purge with a part of the $O_2$ enriched product gas reduced oxygen recovery. In order to overcome this constraint, pressurization with intermediate gas is proposed in this study.

**Table 1** Partial parameters of adsorbent column and particle

| Adsorbent column | | Adsorbent particle | |
| --- | --- | --- | --- |
| $P_H$ (kPa) | 240 | $C_s$ (J kg$^{-1}$ K$^{-1}$) | 1172 |
| $P_{RE}$ (kPa) | 180–200 | $d_p$ (m) | 0.0005 |
| $P_{IPP}$ (kPa) | 80–110 | $\rho_p$ (kg m$^{-3}$) | 1035 |
| $P_L$ (kPa) | 60–80 | $\rho_b$ (kg m$^{-3}$) | 589.46 |
| $y_F$ | 0.21 | $\varepsilon_b$ | 0.52 |
| $y_{RE}$ | 0.45–0.74 | $\varepsilon_p$ | 0.33 |
| $d_{in}$ (m) | 0.03 | $\varepsilon_t$ | 0.68 |
| $l$ (m) | 0.24 | | |
| $L$ (m) | 0.28 | | |
| $T_F$ (K) | 289.15 | | |
| $T_{RE}$ (K) | 289.15 | | |
| $T_W$ (K) | 289.15 | | |

The cyclic sequence of the RVPSA process with intermediate gas pressurization is depicted in Fig. 1. The arrows represent the direction of gas flow. The cycle consisted of (i) co-current pressurization (PR) with feed gas, (ii) selective adsorption (AD) of $N_2$ from a compressed air stream to produce an oxygen enriched gas, (iii) intermediate gas recovery step (RE), in which the feed end was closed and the product end was opened (the useful gas collected after the AD step was called as intermediate gas in this work because the oxygen purity of these gases was <90%), (iv) countercurrent depressurization (CD) of column to desorption pressure, (v) intermediate gas pressurization from product end (IPP), and the repetition of the cycle. The $N_2$ enriched effluent gases from the CD step (iv) were wasted.

### 2.3 RVPSA setup

Figure 2 is a schematic of the RVPSA experimental setup. It consisted of a single adsorbent column (containing 0.1 kg of LiLSX). Aluminum oxide was used to remove the water vapor and carbon dioxide from compressed air at the feed end of the adsorbent column. The amount and diameter of aluminum oxide was 0.02 kg and 0.001 m, respectively. An intermediate gas tank 14 (the tank volume was 0.15 L) was arranged to collect the intermediate gas after the AD step (ii) and throttle 10 was designed to control the oxygen purity and pressure of intermediate gas. Consequently, the pressure in the column and intermediate tank 14 was incomplete equalization at end of the RE step (iii). The stored gas in intermediate tank 14 was used to pressurize from the product end after the CD step (iv). Oxygen enriched product gas was withdrawn through product tank 15. In addition, a dual-use tank design (shown as Fig. S1 in the Supporting Information) can improve the utilization of the tank 14 and tank 15, and simplify the RVPSA system. Notably, the RVPSA experimental setup implemented with an additional vacuum pump was just for
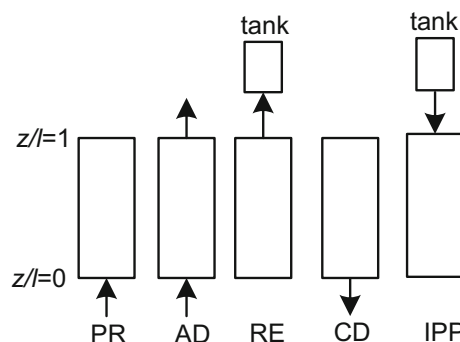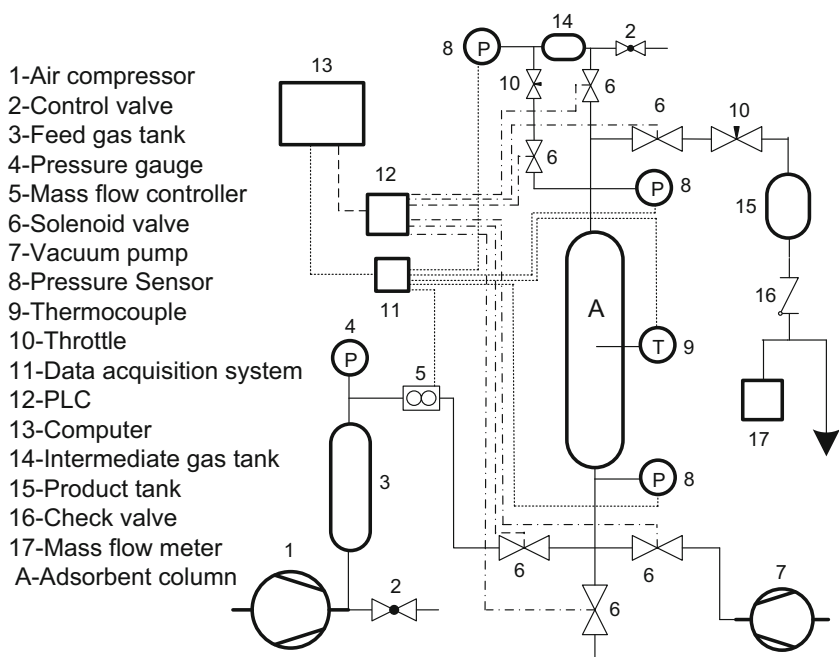


**Fig. 1** Cyclic sequence of the RVPSA process with intermediate gas pressurization

Fig. 2 Schematic of the
RVPSA experimental setup



1-Air compressor
2-Control valve
3-Feed gas tank
4-Pressure gauge
5-Mass flow controller
6-Solenoid valve
7-Vacuum pump
8-Pressure Sensor
9-Thermocouple
10-Throttle
11-Data acquisition system
12-PLC
13-Computer
14-Intermediate gas tank
15-Product tank
16-Check valve
17-Mass flow meter
A-Adsorbent column

experimental study. And a miniature air scroll integrated vacuum and compressor should be applied in real oxygen concentrator products.

Oxygen purity, flow rate of product and other process parameters were measured using different sensors. Moreover, standard deviations of the results were calculated by repeating the experiment three times.

## 3 Mathematical models

### 3.1 Governing equations

The main assumptions of the mathematical model used to simulate the process were: (1) ideal gas behavior; (2) the feed gas was approximated as a mixture of nitrogen and oxygen only in the ratio of 79:21; (3) negligible radial concentration and temperature gradients; (4) uniform particle size and cross-sectional void fraction; (5) adsorption equilibrium described by multicomponent Langmuir isotherm; (6) pressure drop described by Ergun's equation; (7) negligible wall heat conduction and wall external convective heat transfer resistance.

According to these assumptions, the model equations can be written as follows: Gas phase mass balance for component $i$:

$$\varepsilon_t \frac{\partial c_i}{\partial t} - \varepsilon_b D_{ax} \frac{\partial^2 c_i}{\partial z^2} + \varepsilon_b \frac{\partial (u c_i)}{\partial z} + (1 - \varepsilon_b) \rho_p \frac{\partial q_i}{\partial t} = 0 \qquad (1)$$

The axial dispersion coefficient ($D_{ax}$) varies along the length of column following the correlation (Langer et al. 1978; Ruthven 1984; Rama Rao and Farooq 2014):

$$D_{ax} = \gamma_1 D_m + \frac{u d_p}{Pe_\infty \left(1 + \gamma_1 D_m / (u d_p)\right)} \qquad (2)$$

$$\gamma_1 = 0.45 + 0.55 \varepsilon_b \qquad (3)$$

$$Pe_\infty = 3.35 \frac{d_p}{2}, \ d_p \le 0.003 \text{ m} \qquad (4)$$

where the molecular diffusion coefficient $D_m$ is estimated from the Chapman–Enskog equation.

The adsorbed phase mass balance for component $i$ (LDF model):

$$\frac{\partial q_i}{\partial t} = k_i (q_i^* - q_i) \qquad (5)$$

where the LDF mass transfer coefficient for adsorbate $i$ can be estimated using the following simplified model (Ruthven 1984):

$$k_i = \frac{60 D_e}{d_p^2} \frac{c_0}{q_0}, \ D_e = \frac{\varepsilon_p}{\tau_p} \left( \frac{1}{\frac{1}{D_K} + \frac{1}{D_m}} \right) \qquad (6)$$

Adsorption equilibrium (Young and Crowell 1962; Yang 2003):

$$q_i^* = \frac{q_s b_i P_i}{1 + \sum_{k=1}^{2} b_k P_k}, \ b_i = b_i^0 \exp\left(\frac{\Delta H_i}{R T_f}\right) \qquad (7)$$

Gas phase heat balance:

$$\varepsilon_t \rho_f C_f \frac{\partial T_f}{\partial t} + \varepsilon_b \rho_f C_f \frac{\partial (T_f u)}{\partial z} = \varepsilon_b K_f \frac{\partial^2 T_f}{\partial z^2}$$
$$+ (1 - \varepsilon_b) \frac{6 h_f}{d_p} (T_s - T_f)$$
$$- \frac{4 h_w}{d_{in}} (T_f - T_w) \qquad (8)$$

The gas–solid heat transfer coefficient $h_f$ and the internal convective gas-wall heat transfer coefficient $h_w$ were obtained from the Nusselt number $Nu$ ($=hd_{in}/K_f$) by the following correlation. The gas–solid heat transfer coefficient $h_f$ was in the presence of gas phase mass axial dispersion (Wakao et al. 1979):

$$Nu = 2.0 + 1.1\left(Re^{0.6} Pr^{1/3}\right) \tag{9}$$

Internal convective gas-wall heat transfer coefficient $h_w$ (Lopes et al. 2011):

$$Nu = 140 + 0.013396 \frac{d_{in}^2}{d_p K_f} Re \tag{10}$$

Solid phase heat balance:

$$(1 - \varepsilon_t)\rho_p C_s \frac{\partial T_s}{\partial t} = (1 - \varepsilon_b)K_s \frac{\partial^2 T_s}{\partial z^2}$$
$$+ (1 - \varepsilon_b)\frac{6h_f}{d_p}(T_f - T_s)$$
$$+ \rho_p(1 - \varepsilon_b)\sum_{i=1}^{2}\left(\Delta H_i \frac{\partial q_i}{\partial t}\right) \tag{11}$$

The adsorption heat $\Delta H_i$ of component $i$ at an adsorbate loading of $q_i^*$ is given by (Ruthven et al. 1994; Sircar 1999):

$$\left[\frac{\partial \ln(P)}{\partial T_f}\right]_{q_i^*} = -\frac{\Delta H_i}{RT_f^2} \tag{12}$$

Column pressure drop (Ergun 1952):

$$\frac{\partial P}{\partial z} = -\frac{150\mu}{d_p^2}\frac{(1 - \varepsilon_b)^2}{\varepsilon_b^3}u - \frac{1.75\rho_f}{d_p}\frac{(1 - \varepsilon_b)}{\varepsilon_b^3}u^2 \tag{13}$$

### 3.2 Model parameters

The partial parameters of the adsorbent column and particle used in the model are listed in Table 1.

Isotherms for LiLSX pellets used in the present simulations are shown in Fig. S2 in the Supporting Information and the isotherm parameters are listed in Table 2.

### 3.3 Initial and boundary conditions

The initial conditions and boundary conditions for each step are showed in Table 3.

### 3.4 Method of solution

The mathematical model for the simulations of the process described above was solved by self-prepared solver using MATLAB R2009a which used the control volume method.

**Table 2** Values of Langmuir isotherm parameters

| Adsorbate | $q_s$ (mol kg$^{-1}$) | $b_i^0$ (kPa$^{-1}$) | $\Delta H_i$ (J mol$^{-1}$) |
|---|---|---|---|
| O$_2$ | 2.15 | $2.4180 \times 10^{-6}$ | 14,661.44 |
| N$_2$ | 2.15 | $2.8127 \times 10^{-7}$ | 25,451.65 |

To obtain the numerical solutions of the partial differential governing equations, the method of upwind differencing scheme on finite elements was preferred to discretize the axial distance of the adsorption bed into 102 nodes with second-order approximation accuracy. In addition, a 0.01 s time step size was used for the simulations. A change in oxygen purity by ≤0.01% in two consecutive cycles was used as the criteria to confirm the cyclic steady state. The simulations of the feed pressurization (or depressurization) steps were performed using a parabolic exaltation (or decay) function until a pre-defined pressure was achieved.

## 4 Results and discussion

### 4.1 Model validation

Figure 3 shows the pressure change of adsorption column at feed end during the RVPSA process with intermediate gas pressurization. As can be seen from Fig. 3, the change of the pressure in experiment was consistent with the one in simulation in four steps (PR, AD, RE, and IPP step) except the CD step. However, the pressure errors of the CD step are not caused large changes of the process performance because of same desorption pressure.

Table 4 shows the comparison of experimental and simulated process performance (at steady state operation) during the RVPSA process with intermediate gas pressurization. Table 4 showed that the relative deviation of oxygen recovery and the relative error of BSF were less than 2 and 3%, respectively. These errors are acceptable for a PSA oxygen production process.

Figure 4 shows the cyclic profiles of column mid-point gas temperature during the RVPSA process with intermediate gas pressurization. The gas temperature rose rapidly during the PR step and dropped dramatically during the CD step. The differences between the simulation profile and experimental points were within 2 °C. The change of gas temperature was approximately 9 °C during a cycle. The maximum gas temperature was reached at the end of the AD step and the minimum gas temperature was reached at the end of the CD step.

The above comparisons and analysis show that the model can give a favorable prediction. Then, using the model to study the RVPSA process was convincing.

**Table 3** Initial conditions and boundary conditions for the simulations (Lopes et al. 2012)

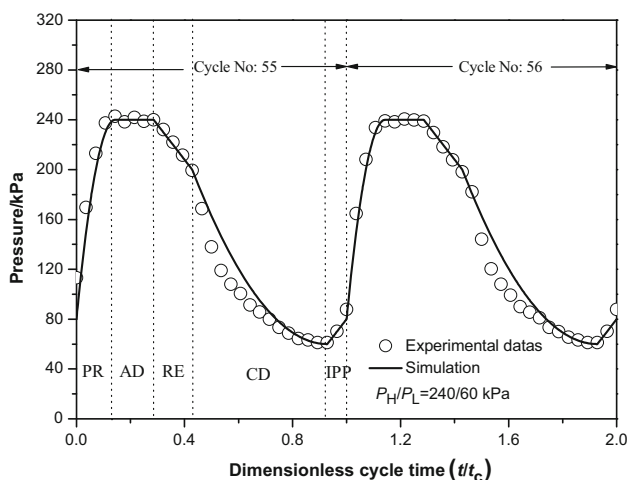| Initial conditions $y(z) = 0.21$; $P(z) = 101.325$ kPa; $T_f(z) = T_s(z) = 289.15$ K | | |
|---|---|---|
| Step | $z = 0$ (inlet) | $z = l$ (outlet) |
| PR | $D_{ax} \frac{\partial y}{\partial z} = -u(y_F - y)$ | $u = 0$ |
| | $K_f \frac{\partial T_f}{\partial z} = -u \rho_f C_f (T_F - T_f)$ | $\frac{\partial y}{\partial z} = 0$ |
| | | $\frac{\partial T_f}{\partial z} = 0$ |
| | | $P = P_H + (P_{IPP} - P_H)(t/t_{PR} - 1)^2$ |
| AD | $u = u_{in}$ | $\frac{\partial y}{\partial z} = 0$ |
| | $D_{ax} \frac{\partial y}{\partial z} = -u(y_F - y)$ | $\frac{\partial T_f}{\partial z} = 0$ |
| | $K_f \frac{\partial T_f}{\partial z} = -u \rho_f C_f (T_F - T_f)$ | |
| | $P = P_H$ | |
| RE | $u = 0$ | $\frac{\partial y}{\partial z} = 0$ |
| | $\frac{\partial y}{\partial z} = 0$ | $\frac{\partial T_f}{\partial z} = 0$ |
| | $\frac{\partial T_f}{\partial z} = 0$ | |
| | $P = P_H + (P_{RE} - P_H)(t/t_{RE})$ | |
| CD | $\frac{\partial y}{\partial z} = 0$ | $u = 0$ |
| | $\frac{\partial T_f}{\partial z} = 0$ | $\frac{\partial y}{\partial z} = 0$ |
| | | $\frac{\partial T_f}{\partial z} = 0$ |
| | | $P = P_L + (P_{RE} - P_L)(t/t_{CD} - 1)^2$ |
| IPP | $u = 0$ | $D_{ax} \frac{\partial y}{\partial z} = -u(y_{RE} - y)$ |
| | $\frac{\partial y}{\partial z} = 0$ | $K_f \frac{\partial T_f}{\partial z} = -u \rho_f C_f (T_{RE} - T_f)$ |
| | $\frac{\partial T_f}{\partial z} = 0$ | |
| | $P = P_L + (P_{IPP} - P_L)(t/t_{IPP})$ | |



**Fig. 3** Pressure histories of adsorption column at feed end during the RVPSA process with intermediate gas pressurization

## 4.2 Effect of intermediate gas pressurization step on oxygen production process

Figure 5 shows the effect of cycle time on experimental oxygen purity of the product during the RVPSA cycle with intermediate gas pressurization and without intermediate

gas pressurization. And there is same feed flow-rate for the two types (with and without intermediate gas pressurization) of RVPSA processes. With the adsorption and desorption pressures of 240 and 60 kPa, respectively, the oxygen purity of product at a constant flow rate of 0.75 L min⁻¹ improved with the increase of cycle time, and then decreased with the increase of cycle time. The oxygen purity of the product reached a maximum at an optimum cycle time. The optimum cycle time was 7 s for both cycles with intermediate gas pressurization and without intermediate gas pressurization. The individual step cycle times for this case were 1, 1, 1, 3.5, and 0.5 s, respectively, for steps i ($t_{PR}$), ii ($t_{AD}$), iii ($t_{RE}$), iv ($t_{CD}$), and v ($t_{IPP}$) of the cycle with intermediate gas pressurization. The individual step cycle times were 1.5, 1, 1, and 3.5 s, respectively, for steps i ($t_{PR}$), ii ($t_{AD}$), iii ($t_{RE}$), and iv ($t_{CD}$) of the cycle without intermediate gas pressurization.

In addition, as seen from Fig. 5, intermediate gas pressurization from product end could effectively improve the oxygen purity of the product during the RVPSA process. The oxygen purity of the product during the cycle with intermediate gas pressurization was up to 90.3% at optimum cycle time, and improved by 15.85% compared with the cycle without intermediate gas pressurization. The steady state

**Table 4** Experimental and simulated process performance under different cycle times

| $t_C$(s) | Oxygen recovery (∼90% O₂ product) (%) | | | BSF (∼90% O₂ product) (kg TPD⁻¹) | | |
|---|---|---|---|---|---|---|
| | Exp. | Sim. | Deviation (%) | Exp. | Sim. | Relative error (%) |
| 5 | 22.12 | 23.49 | 1.37 | 114.18 | 112.13 | 1.79 |
| 6 | 26.25 | 27.68 | 1.43 | 94.06 | 92.09 | 2.09 |
| 7 | 29.45 | 30.93 | 1.48 | 82.84 | 81.26 | 1.91 |
| 8 | 29.85 | 31.56 | 1.71 | 86.35 | 84.14 | 2.56 |
| 9 | 30.25 | 31.81 | 1.56 | 94.02 | 92.01 | 2.13 |
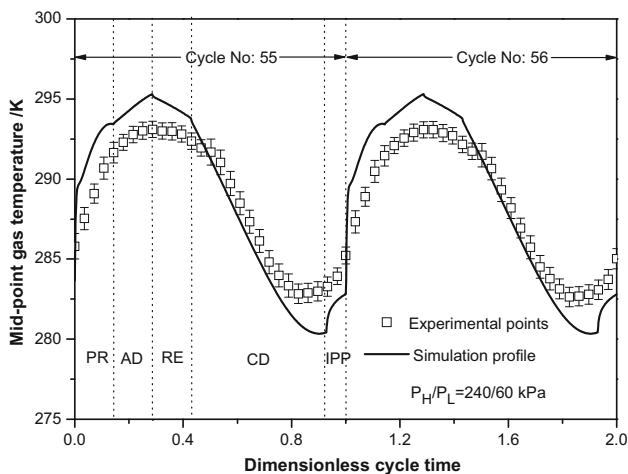


**Fig. 4** Cyclic profiles of column mid-point gas temperature during the RVPSA process with intermediate gas pressurization; *error bar* represents standard deviation
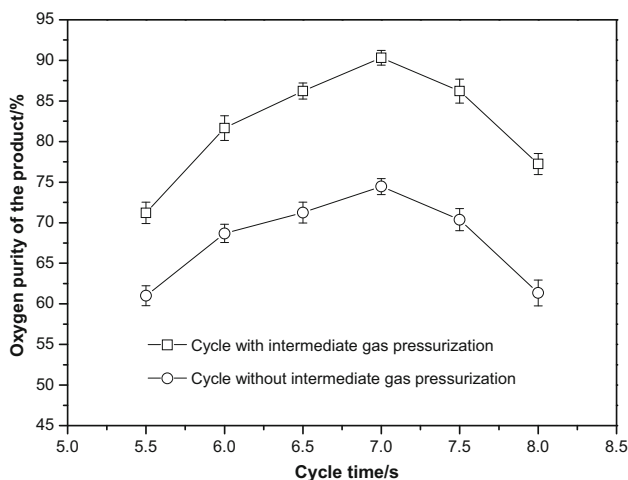


**Fig. 5** Effect of cycle time on experimental oxygen purity of the product during the RVPSA cycle with intermediate gas pressurization and without intermediate gas pressurization; the pressure and oxygen purity of intermediate gas before pressurization were 165 kPa and 72 ± 2%, respectively; *error bar* represents standard deviation

column profiles of gas phase O₂ mol fraction, N₂ mol fraction, and specific N₂ loading at the end of each step as functions of dimensionless column height (z/l) for the RVPSA cycle with intermediate gas pressurization and without

intermediate gas pressurization are showed in Fig. S4 in the Supporting Information. The simulation results showed that the gas phase O₂ mol fraction of the product end could be effectively improved during the RVPSA cycle with intermediate gas pressurization, which was beneficial to produce high oxygen purity of the product during the AD step.

The effects of pressurization with different oxygen purities of intermediate gas on experimental oxygen purity of the product are shown as Fig. 6, where the intermediate gas pressure before pressurization and the product flow rate are 165 kPa and 0.75 L min⁻¹, respectively. Figure 6 showed that the pressurization with higher oxygen purity of intermediate gas results in higher oxygen purity of the product. When the oxygen purity of intermediate gas was more than 70%, oxygen purity of the product was ∼90%. The effects of pressurization with different oxygen purities of intermediate gas on gas phase concentration and temperature distribution at the end of IPP step are shown as Fig. S5 in the Supporting Information. The figures showed that the pressurization with higher oxygen purity of intermediate gas can push N₂ mass transfer zones closer to the feed end and make lower gas temperature at product end, which confirmed the more beneficial effects for oxygen purity of product by pressurization with higher oxygen purity of intermediate gas.
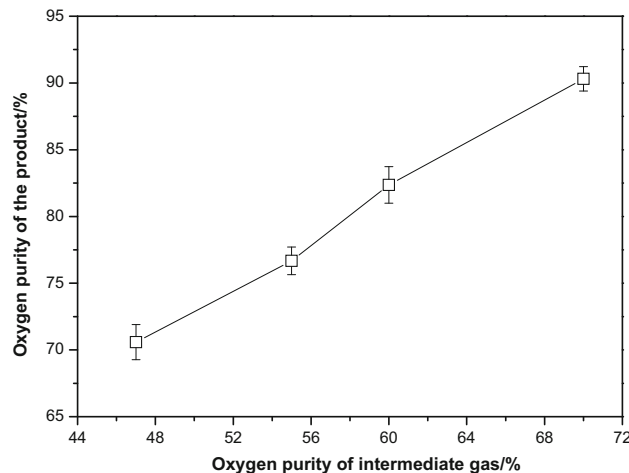


**Fig. 6** Effect of oxygen purity of intermediate gas on experimental oxygen purity of the product; *error bar* represents standard deviation
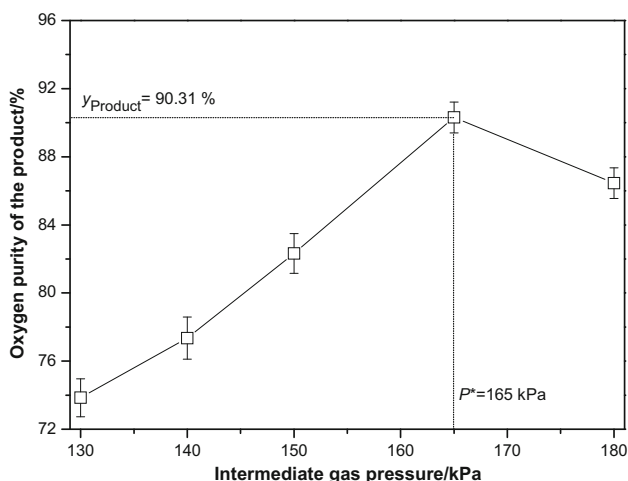
**Fig. 7** Effect of intermediate gas pressure on experimental oxygen purity of the product; *error bar* represents standard deviation



**Fig. 9** Effect of desorption pressure on experimental oxygen recovery of the RVPSA system
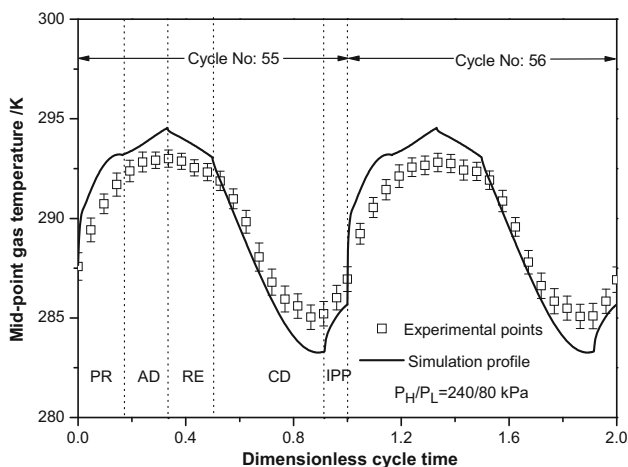


**Fig. 8** Mid-point column gas temperature profiles of the RVPSA process with desorption pressure of 80 kPa; *error bar* represents standard deviation



**Fig. 10** Effect of desorption pressure on experimental BSF of the RVPSA system

The effects of intermediate gas pressure before pressurization on experimental oxygen purity of the product are shown as Fig. 7, where the oxygen purity of intermediate gas before pressurization and the product flow rate are $72 \pm 2\%$ and $0.75$ L min$^{-1}$, respectively. Figure 7 showed that the $\sim 90\%$ O$_2$ product can be obtained at a suitable intermediate gas pressure $P^*$ ($P^* = 165$ kPa). When the intermediate gas pressure exceeded or was less than $P^*$, the oxygen purity of the product will decrease. The effects of intermediate gas pressure before pressurization on the gas phase concentration and temperature distribution at the end of IPP step are shown as Fig. S6 in the Supporting Information. The figures showed that the N$_2$ mass transfer zones were pushed closer to the feed end and the gas phase temperature was higher at the feed end by pressurization
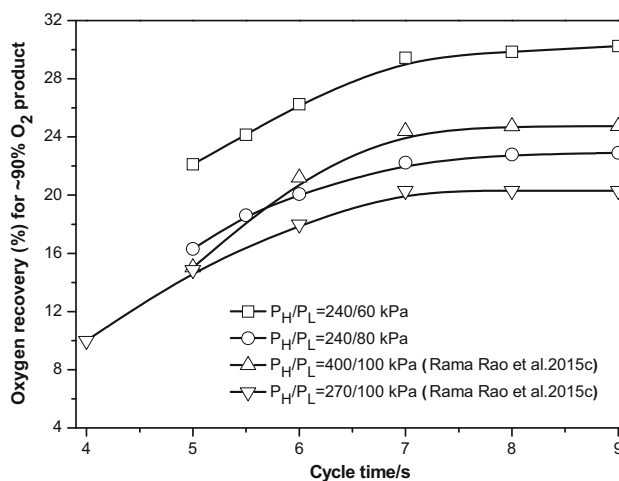
with intermediate at $P^*$. Then higher oxygen concentration and lower gas temperature was obtained near the product end, which was favorable to produce higher oxygen purity of the product.

## 4.3 Effect of desorption pressure on process performance

The effects of desorption pressure on the performance of the RVPSA process with intermediate gas pressurization were also experimentally investigated, which has much practical importance for prompting its applications. The mid-point column gas temperature profiles during the last two cycle with desorption pressure of 80 kPa are shown in Fig. 8. The mid-point column gas temperature profiles

**Table 5** Performance of nitrogen adsorbents for two different RPSA systems

| | $d_p \times 10^4$ (m) | $S_{12}$ (291.15 K and 101.325 kPa) | $\Delta H_i$ (J mol$^{-1}$) | Manufacturer |
|---|---|---|---|---|
| Our | ∼5.0 | 8.7 | 14,661.44($O_2$)<br>25,451.65($N_2$) | Jianlong Micro-nano Novel Materials Co., LTD (China) |
| Rama Rao | ∼5.6 | ∼9.8 (Wu et al. 2014a) | 13,478.44($O_2$)<br>24,570.95($N_2$) (Wu et al. 2014b) | Zeochem Corporation |

**Table 6** Comparison of process parameters for two different RPSA systems (Rama Rao et al. 2014c, 2015c)

| | Amount of adsorbent (kg) | $t_C$ (s) | Average feed flow rate (L min$^{-1}$) | Average product flow rate (L min$^{-1}$) |
|---|---|---|---|---|
| Our | 0.1 | 7 | ∼10 | 0.75 |
| Rama Rao | 0.148 | 5.5 | ∼30 | 2.2 |

during the last two cycles with desorption pressure of 60 kPa were previously shown in Fig. 4. The change of gas temperature profiles during a cycle was similar for different desorption pressures. By contrast, the minimum gas temperature was smaller when the desorption pressure was lower because of smaller $N_2$ adsorption capacity.

The effects of desorption pressure on experimental oxygen recovery of the RVPSA system for ∼90% $O_2$ product are shown in Fig. 9. Figure 9 also shows the comparison of experimental oxygen recovery results from Rama Rao et al. (2015c) and our study. As seen from Fig. 9, the oxygen recovery gradually increased with the increase of the cycle time, and then gradually reached a stable value. The oxygen recovery could effectively improve by lowering desorption pressure. With the adsorption and desorption pressures of 240 and 60 kPa, the oxygen recovery was 29.45%, and higher by 5% than the Skarstrom-based RPSA system constructed by Rama Rao et al. (2015c).

The effects of desorption pressure on experimental BSF of the RVPSA system are shown in Fig. 10. The figure also showed the comparison of experimental BSF results from Rama Rao et al. (2015c) and ours. As shown in Fig. 10, the BSF could be reduced by lowering cycle time, but cannot be indefinitely reduced by lowering cycle time. This trend was similar to the results in the literature (Chai et al. 2011; Rama Rao et al. 2014c, 2015a, b, c). When the adsorption pressure was 240 kPa and desorption pressure was 60 kPa, a minimum BSF of 82.84 kg TPD$^{-1}$ with an optimum cycle time of 7 s could be achieved during the process. However, the BSF of this was almost two times that of the Skarstrom-based RPSA system constructed by Rama Rao et al. (2014c, 2015c). Some possible reasons exist for the higher BSF. Performance parameters of the adsorbents used in RPSA system constructed by Rama Rao et al.

(2014c, 2015c) and the RVPSA system are shown as Table 5.

Table 5 shows that, some significant performance differences existed between the two nitrogen adsorbents. The effects of adsorbent selectivity on the process performance are significant (Wu et al. 2016). The lower adsorbent selectivity and higher heat of adsorption were main reasons for higher BSF of the RVPSA process. Another key clue for the difference of BSF was given by process parameters, as shown in Table 6. As seen from Table 6, the longer cycle time and lower product flow rate were important reasons for higher BSF of the RVPSA process. If the RVPSA system was applied at high altitudes, the desorption time may decrease from 3.5 s to 1 s and thus the cycle optimum time decreases from 7 to 4.5 s and the BSF reduces from 82.84 to 53.26 kg TPD$^{-1}$ with an oxygen recovery of ∼30%. Then the performance is comparable with the RPSA system.

## 5 Conclusions

A novel RVPSA process with intermediate gas pressurization for producing oxygen is proposed for improving performance of the miniature oxygen concentrator based RPSA technology. The effect of intermediate gas pressurization step and desorption pressure on performance of the process were evaluated through experiments and simulations. The RVPSA process is featured by low adsorption pressure, and then the adverse effects induced by high adsorption pressure of the RPSA system may be weakened.

Results showed that pressurization with intermediate gas from product end could effectively improve the oxygen purity of the product. The pressure and oxygen purity of intermediate gas before pressurization were key parameters to influence the oxygen purity of the product. The test unit

for the process produced 0.75 L min$^{-1}$ of 90% O$_2$ from compressed air. When the adsorption pressure was 240 kPa and the desorption pressure was 60 kPa, the minimum BSF with 29.45% of oxygen recovery for ~90% O$_2$ product was 82.84 kg TPD$^{-1}$. The lower adsorbent selectivity, longer cycle time and smaller product flow rate were the cause of higher BSF. The BSF could be effectively reduced by decreasing the desorption pressure. In addition, the oxygen recovery could improve by lowering desorption pressure.

# References

Alpay, E., Kenney, C.N., Scott, D.M.: Adsorbent particle size effects in the separation of air by rapid pressure swing adsorption. Chem. Eng. Sci. **49**, 3059–3075 (1994)

Chai, S.W., Kothare, M.V., Sircar, S.: Rapid pressure swing adsorption for reduction of bed size factor of a medical oxygen concentrator. Ind. Eng. Chem. Res. **50**, 8703–8710 (2011)

Chai, S.W., Kothare, M.V., Sircar, S.: Numerical study of nitrogen desorption by rapid oxygen purge for a medical oxygen concentrator. Adsorption **18**, 87–102 (2012)

Chai, S.W., Kothare, M.V., Sircar, S.: Efficiency of nitrogen desorption from LiX zeolite by rapid oxygen purge in a pancake adsorber. AIChE J **59**, 365–368 (2013)

Drevitson, K.C., Carella, P.F., Carella, R.L., Clemente, M.A., Johnson, R.D.: Integrated shop vacuum and air compressor system. U.S. Patent, 119,016 (2007)

Ergun, S.: Fluid flow through packed columns. Chem. Eng. Prog. **48**, 89–94 (1952)

Hu, Z.M, Chen, S.H., Xu, Y.D., Yang, S.J., Chen, R.: Direct attach explosion proof oil-free scroll vacuum compressor. C.N. Patent, 101,509,489 (2009)

Huang, W.C., Chou, C.T.: Comparison of radial and axial flow rapid pressure swing adsorption processes. Ind. Eng. Chem. Res. **42**, 1998–2006 (2003)

Langer, G., Roethe, A., Roethe, K.P., Gelbin, D.: Heat and mass-transfer in packed-beds. 3. Axial mass dispersion. Int. J. Heat Mass Transf **21**, 751–759 (1978)

Leavitt, F.W.: Improved air separation pressure swing adsorption process. E.P. Patent, 461,478 (1991)

Liu, Y.S., Zheng, X.G., Dai, R.F.: Numerical study of flow maldistribution and depressurization strategies in a small-scale axial adsorber. Adsorption **20**, 757–768 (2014)

Lopes, F.V.S., Grande, C.A., Rodrigues, A.E.: Activated carbon for hydrogen purification by pressure swing adsorption: multicomponent break through curves and PSA performance. Chem. Eng. Sci. **66**, 303–317 (2011)

Lopes, F.V.S., Grande, C.A., Rodrigues, A.E.: Fast-cycling VPSA for hydrogen purification. Fuel **93**, 510–523 (2012)

Rama Rao, V., Farooq, S.: Experimental study of a pulsed pressure swing adsorption process with very small 5A zeolite particles for oxygen enrichment. Ind. Eng. Chem. Res. **53**, 13157–13170 (2014)

Rama Rao, V., Farooq, S., Krantz, W.B.: Design of a two-step pulsed pressure swing adsorption based oxygen concentrator. AIChE J **56**, 354–370 (2010)

Rama Rao, V., Kothare, M.V., Sircar, S.: Numerical simulation of rapid pressurization and depressurization of a zeolite column using nitrogen. Adsorption **20**, 53–60 (2014a)

Rama Rao, V., Chai, S.W., Kothare, M.V., Sircar, S.: Highlights of non-equilibrium, non-isobaric, non-isothermal desorption of nitrogen from a LiX zeolite column by rapid pressure reduction and rapid purge by oxygen. Adsorption **20**, 477–481 (2014b)

Rama Rao, V., Kothare, M.V., Sircar, S.: Novel design and performance of a medical oxygen concentrator using a rapid pressure swing adsorption concept. AIChE J. **60**, 3330–3335 (2014c)

Rama Rao, V., Kothare, M.V., Sircar, S.: Anatomy of a rapid pressure swing adsorption process performance. AIChE J **61**, 2008–2015 (2015a)

Rama Rao, V., Wu, C.W., Kothare, M.V., Sircar, S.: Comparative performances of two commercial samples of LiLSX zeolite for production of 90% oxygen from air by a novel rapid pressure swing adsorption system. Sep. Sci. Technol. **50**, 1447–1452 (2015b)

Rama Rao, V., Kothare, M.V., Sircar, S.: Performance of a medical oxygen concentrator using rapid pressure swing adsorption process: effect of feed air pressure. AIChE J. **62**, 1212–1215 (2015c)

Rege, S.U., Yang, R.T.: Limits for air separation by adsorption with LiX Zeolite. Ind. Eng. Chem. Res. **36**, 5358–5365 (1997)

Ruthven, D.M.: Principles of Adsorption and Adsorption Processes. Wiley, New York (1984)

Ruthven, D.M., Farooq, S., Knaebel, K.S.: Pressure Swing Adsorption. VCH, New York (1994)

Shen, G.H., Xie, K.N., Yan, Y.L., Jing, D., Tang, C., Wu, X.M., Liu, J., Sun, T., Zhang, J.B., Luo, E.P.: The role of oxygen-increased respirator in humans ascending to high altitude. Biomed. Eng. Online. **11**, 49–56 (2012)

Shen, G.H., Wu, X.M., Tang, C., Yan, Y.L., Liu, J., Guo, W., Jing, D., Lei, T., Tian, Y., Xie, K.M., Luo, E.P., Zhang, J.B.: An oxygen enrichment device for lowlanders ascending to high altitude. Biomed. Eng. Online. **12**, 100–108 (2013)

Sircar, S.: Gibbsian surface excess for gas adsorption-revisited. Ind. Eng. Chem. Res. **38**, 3670–3682 (1999)

Sircar, S., Hanley, B.F.: Production of oxygen enriched air by rapid pressure swing adsorption. Adsorption **1**, 313–320 (1995)

Wakao, N., Kaguei, S., Funazkri, T.: Effect of fluid dispersion coefficients on particle to fluid heat transfer coefficients in packed beds. Chem. Eng. Sci. **34**, 325–336 (1979)

Windsor, J.S., Rodway, G.W.: Supplemental oxygen and sleep at altitude. High Alt. Med. Biol. **7**, 307–311 (2006)

Wu, C.W., Kothare, M.V., Sircar, S.: Model analysis of equilibrium adsorption isotherms of pure N$_2$, O$_2$, and their binary mixtures on LiLSX zeolite. Ind. Eng. Chem. Res. **53**, 12428–12434 (2014a)

Wu, C.W., Kothare, M.V., Sircar, S.: Equilibrium adsorption isotherms of pure N$_2$ and O$_2$ and their binary mixtures on LiLSX zeolite: experimental data and thermodynamic analysis. Ind. Eng. Chem. Res. **53**, 7195–7201 (2014b)

Wu, C.W., Rama Rao, V., Kothare, M.V., et al.: Experimental study of a novel rapid pressure-swing adsorption based medical oxygen concentrator: effect of the adsorbent selectivity of N$_2$ over O$_2$. Ind. Eng. Chem. Res. **55**, 4676–4681 (2016)

Yang, R.T.: Adsorbents: Fundamentals and Applications. Wiley, New York (2003)

Young, D.M., Crowell, A.D.: Physical Adsorption of Gases. Butterworths, London (1962)